

# Medium Effects on Charmonium Production at LHC

Kai Zhou<sup>1</sup>, Nu Xu<sup>2,3</sup>, Zhe Xu<sup>1</sup>, Pengfei Zhuang<sup>1</sup>

<sup>1</sup>*Physics Department, Tsinghua University and Collaborative Innovation Center of Quantum Matter, Beijing 100084, China*

<sup>2</sup>*Nuclear Science Division, Lawrence Berkeley National Laboratory, Berkeley, CA 94720, USA*

<sup>3</sup>*Key Laboratory of Quark and Lepton Physics (MOE) and Institute of Particle Physics, Central China Normal University, Wuhan 430079, China*

(Dated: June 4, 2014)

We investigate with a transport approach the cold and hot nuclear matter effects on the charmonium transverse momentum distributions in relativistic heavy ion collisions. The newly defined nuclear modification factor  $r_{AA} = \langle p_T^2 \rangle_{AA} / \langle p_T^2 \rangle_{pp}$  and elliptic flow  $v_2$  for  $J/\psi$  are sensitive to the nature of the hot medium and the thermalization of heavy quarks. From SPS through RHIC to LHC colliding energies, we observe dramatic changes in the centrality dependence of  $r_{AA}$ . We find that at LHC energy, the finally observed charmonia are dominated by the regeneration from thermalized heavy quarks.

PACS numbers: 25.75.-q, 12.38.Mh, 24.85.+p

## I. INTRODUCTION

Charmonium production has long been considered as a clean probe for the Quantum Chromodynamics (QCD) matter formed in heavy ion collisions at relativistic energy [1], due to the color screening of heavy quark potential at finite temperature [2, 3]. When the temperature of the medium becomes higher than the charmonium dissociation temperature  $T_d$ , the initially produced charmonia will be destroyed. It is called the anomalous suppression [4]. Therefore the comparison of the final yield of charmonia from heavy ion collisions to that from the corresponding nucleon-nucleon collisions can be used to extract the medium properties in high-energy nuclear collisions [1]. This anomalous suppression induced by the hot nuclear matter effect explains well the experimentally observed charmonium suppression at the Super Proton Synchrotron (SPS) [5, 6]. However, color screening is not the only hot medium effect in high-energy nuclear collisions. Once the energy is sufficiently high, such as the collisions at the Relativistic Heavy Ion Collider (RHIC) and the Large Hadron Collider (LHC), many charm quarks are produced [7, 8]. The initially uncorrelated charm quarks  $c$  and  $\bar{c}$  can recombine into a charmonium. This process is called regeneration [9–11]. In high-energy nuclear collisions, these two effects are co-existing and their relative strength is energy dependent. At RHIC it turns out that both suppression and regeneration processes are important for understanding the charmonium production [12, 13].

Even before the formation of Quark-Gluon Plasma (QGP), the cold nuclear matter effects affect the charmonium production. Usually three effects are considered in the literatures: (1) The change in the parton distribution function in nucleus which controls the initial parton behavior and strongly depends on the collision kinematics. In the small  $x$  region, the nuclear parton distribution function is clearly suppressed compared to that of nucleon. That is called the shadowing effect [14]; (2) Cronin effect [15] which describes the initial gluon multi-scattering with the nucleons prior to any hard scattering and the quarkonium formation. The nature of such collisions can be described as Brownian motion. As a result the transverse momentum distribution of the produced char-

monia is broadened; and (3) Nuclear absorption via interaction between charmonia and the primary nucleons which leads to the normal suppression of charmonia [16]. Both Cronin effect and nuclear absorption have been studied in p+A collisions [5, 17], while a deep understanding of shadowing effect requires e+p and e+A collisions. In order to understand the charmonium production and extract properties of the medium created in high-energy nuclear collisions, one must take into account both cold and hot nuclear matter effects.

LHC provides new data on the charmonium production in Pb+Pb collisions at colliding energy  $\sqrt{s_{NN}} = 2.76$  TeV [18–21]. At LHC the initially produced charmonia are strongly suppressed by the hotter, larger and longer lived fireball, hence the regeneration becomes the dominant production source. Different from RHIC where the parton longitudinal momentum fraction  $x \gtrsim 0.01$  is located in the interface between shadowing and anti-shadowing [22] regions and therefore the shadowing and anti-shadowing effect is not yet very strong (the ratio of parton distribution function in A+A and p+p collisions is between 0.96 and 1.08 for charmonium transverse momentum  $0 < p_t < 5$  GeV/c, see Fig.7 of Ref.[22]), the collisions at LHC with much smaller  $x$  are in the strong shadowing region [23], and the shadowing effect plays an important role in the study of charmonium production.

In the present study, we will extend our detailed transport approach for charmonium motion in QGP to self-consistently including both the cold and hot nuclear matter effects, and apply it to the charmonium production at LHC energy. The suppression and regeneration mechanisms in the hot medium are reviewed in Section II, and the shadowing effect, the Gaussian smearing treatment for the Cronin effect, and the initial charmonium distribution are focused in Section III. The comparison between the theoretical calculations and the experimental data are shown in Section IV. We summarize our study in Section IV.

## II. HOT NUCLEAR MATTER EFFECT

In order to extract information about the nature of the medium from charmonium production in heavy ion collisions,

the medium created in the initial stage and the charmonia produced in the initial stage and in the medium should be treated both dynamically.

We employ the well tested 2+1 dimensional version [24] of the ideal hydrodynamic equations

$$\partial_\mu T^{\mu\nu} = 0 \quad (1)$$

to simulate the evolution of the almost baryon-free medium created at RHIC and LHC, where  $T_{\mu\nu}$  is the energy-momentum tensor of the medium. The solution of the hydrodynamic equations provides the local temperature and fluid velocity of the medium which will be used in the charmonium regeneration and suppression.

To close the hydrodynamical equations one needs to know the equation of state of the medium. We follow Ref.[25] where the deconfined phase at high temperature is an ideal gas of gluons and massless  $u$  and  $d$  quarks plus 150 MeV massed  $s$  quarks, and the hadron phase at low temperature is an ideal gas of all known hadrons and resonances with mass up to 2 GeV [26]. There is a first order phase transition between these two phases. In the mixed phase, the Maxwell construction is used. The mean field repulsion parameter and the bag constant are chosen as  $K=450$  MeV fm<sup>3</sup> and  $B^{1/4}=236$  MeV to obtain the critical temperature  $T_c = 165$  MeV [25] at vanishing baryon number density.

Taking the initialization in Ref. [27] for the hydrodynamic equations, we get the maximum temperature  $T_0 = 484$  and 430 MeV of the medium at the initial time  $\tau_0 = 0.6$  fm/c, corresponding respectively to the observed charge number density  $dN_{ch}/dy = 1600$  in mid rapidity and 1200 in forward rapidity by the ALICE collaboration [28].

Since a charmonium is so heavy, its equilibrium with the medium can hardly be reached, one usually uses a transport approach to describe the charmonium motion in the medium. The charmonium distribution function  $f_\Psi(\mathbf{x}, \mathbf{p}, t|\mathbf{b})$  in the phase space  $(\mathbf{x}, \mathbf{p})$  at time  $t$  in heavy ion collisions with impact parameter  $\mathbf{b}$  is controlled by the Boltzmann-type equation

$$p^\mu \partial_\mu f_\Psi = -C_\Psi f_\Psi + D_\Psi. \quad (2)$$

Considering the contribution from the feed-down of the excited states  $\psi'$  and  $\chi_c$  to the finally observed  $J/\psi$  [29], we should take into account the transport equations for all the charmonium states  $\Psi = J/\psi, \psi'$  and  $\chi_c$ , when we calculate the  $J/\psi$  distribution. The lose and gain terms  $C_\Psi(\mathbf{x}, \mathbf{p}, t|\mathbf{b})$  and  $D_\Psi(\mathbf{x}, \mathbf{p}, t|\mathbf{b})$  describe the charmonium dissociation and regeneration, and the elastic scattering is neglected since the charmonium mass is much larger than the typical medium temperature. Introducing proper time  $\tau = \sqrt{t^2 - z^2}$ , space rapidity  $\eta = 1/2 \ln[(t+z)/(t-z)]$ , momentum rapidity  $y = 1/2 \ln[(E+p_z)/(E-p_z)]$  and transverse energy  $E_T = \sqrt{E^2 - p_z^2}$  to replace  $t, z, p_z$  and  $E = \sqrt{m^2 + \mathbf{p}^2}$ , the transport equation can be rewritten as

$$\left[ \cosh(y-\eta) \frac{\partial}{\partial \tau} + \frac{\sinh(y-\eta)}{\tau} \frac{\partial}{\partial \eta} + \mathbf{v}_T \cdot \nabla_T \right] f_\Psi = -\alpha_\Psi f_\Psi + \beta_\Psi, \quad (3)$$

where the third term in the square bracket arises from the free streaming of  $\Psi$  with transverse velocity  $\mathbf{v}_T = \mathbf{p}_T/E_T$  which leads to a strong leakage effect at SPS energy [30], and the loss term  $\alpha_\Psi(\mathbf{x}, \mathbf{p}, t|\mathbf{b}) = C_\Psi(\mathbf{x}, \mathbf{p}, t|\mathbf{b})/E_T$  and gain term  $\beta_\Psi(\mathbf{x}, \mathbf{p}, t|\mathbf{b}) = D_\Psi(\mathbf{x}, \mathbf{p}, t|\mathbf{b})/E_T$  are respectively the charmonium dissociation and regeneration rates.

Considering the gluon dissociation  $\Psi + g \rightarrow c + \bar{c}$  as the dominant dissociation process in the hot QGP,  $\alpha$  can be calculated by the gluon momentum integration of the dissociation cross section  $\sigma_{g\Psi}$  multiplied by the thermal gluon distribution  $f_g$  and the flux factor  $F_{g\Psi}$ ,

$$\alpha_\Psi = \frac{1}{2E_T} \int \frac{d^3\mathbf{k}}{(2\pi)^3 2E_g} \sigma_{g\Psi}(\mathbf{p}, \mathbf{k}, T) 4F_{g\Psi}(\mathbf{p}, \mathbf{k}) f_g(\mathbf{k}, T), \quad (4)$$

where  $E_g$  is the gluon energy, the cross section  $\sigma_{g\Psi}$  in vacuum can be derived through the operator production expansion with perturbative Coulomb wave function [31–34], and the cross section at finite temperature is estimated by taking the geometrical relation between the cross section and the average size of the charmonium state,  $\sigma_{g\Psi}(\mathbf{p}, \mathbf{k}, T) = \sigma_{g\Psi}(\mathbf{p}, \mathbf{k}, 0) \langle r_\Psi^2 \rangle(T) / \langle r_\Psi^2 \rangle(0)$ . The averaged radius square  $\langle r_\Psi^2 \rangle$  for the bound state  $\Psi$  can be obtained from the potential model [35, 36], its divergence self-consistently defines a Mott dissociation temperature  $T_d$  which indicates the melting of the bound state due to color screening. The local temperature  $T(\mathbf{x}, t|\mathbf{b})$  and the fluid velocity  $u_\mu(\mathbf{x}, t|\mathbf{b})$  of the medium in the cross section and the gluon thermal distribution come from the solution of the ideal hydrodynamic equations (1).

The regeneration cross section is connected to the dissociation cross section  $\sigma_{g\Psi}$  via the detailed balance between the gluon dissociation and reversed process [12]. To obtain the regeneration rate  $\beta_\Psi$ , we need also the charm quark distribution  $f_c(\mathbf{x}, \mathbf{q}, t|\mathbf{b})$  in the medium. From the experimental data at RHIC and LHC, the observed large quench factor [37, 38] and elliptic flow [39, 40] for charmed mesons indicate that the charm quarks interact strongly with the medium. Therefore, one can reasonably take, as a good approximation, a kinetically thermalized phase space distribution  $f_c$  for charm quarks,  $f_c(\mathbf{x}, \mathbf{q}, t|\mathbf{b}) = 1/(e^{q^\mu u_\mu/T} + 1)$ . Neglecting the creation and annihilation for charm-anticharm pairs inside the medium, the spacial density of charm (anti-charm) quark number  $\rho_c(\mathbf{x}, t|\mathbf{b}) = \int d^3\mathbf{q}/(2\pi)^3 f_c(\mathbf{x}, \mathbf{q}, t|\mathbf{b})$  satisfies the conservation law

$$\partial_\mu (\rho_c u^\mu) = 0 \quad (5)$$

with the initial density determined by the nuclear geometry

$$\rho_c(\mathbf{x}, \tau_0|\mathbf{b}) = \frac{T_A(\mathbf{x}_T) T_B(\mathbf{x}_T - \mathbf{b}) \cosh \eta}{\tau_0} \frac{d\sigma_{pp}^{c\bar{c}}}{d\eta}, \quad (6)$$

where  $T_A$  and  $T_B$  are the thickness functions at transverse coordinate  $\mathbf{x}_T$  defined in the Glauber model [41], and  $d\sigma_{pp}^{c\bar{c}}/d\eta$  is the rapidity distribution of charm quark production cross section in p+p collisions [42–45].

### III. COLD NUCLEAR MATTER EFFECT

The initial condition for the charmonium transport equation (3) can be obtained from a geometrical superposition of p+p collisions, along with the modification from the cold nuclear matter effect. For the charmonium production, the cold nuclear matter effect includes usually the nuclear shadowing [14], Cronin effect [15] and nuclear absorption [16]. At LHC energy, the collision time for two heavy nuclei to pass through each other is much shorter than the charmonium formation time and the QGP formation time, and one can safely neglect the nuclear absorption and just take into account the nuclear shadowing and Cronin effect.

The Cronin effect broadens the momentum of the initially produced charmonia in heavy ion collisions. Before two gluons fuse into a charmonium, they acquire additional transverse momentum via multi-scattering with the around nucleons, and this extra momentum would be inherited by the produced charmonium. Inspired from a random-walk picture, we take a Gaussian smearing [13, 46] for the modified transverse momentum distribution  $\bar{f}_{\Psi}^{pp}(\mathbf{x}, \mathbf{p}, z_A, z_B|\mathbf{b})$

$$\bar{f}_{\Psi}^{pp} = \frac{1}{\pi a_{gN}^2} \int d^2\mathbf{p}'_T e^{-\frac{\mathbf{p}'_T{}^2}{a_{gN}^2}} f_{\Psi}^{pp}(|\mathbf{p}_T - \mathbf{p}'_T|, p_z), \quad (7)$$

where  $l(\mathbf{x}, z_A, z_B|\mathbf{b})$  is the path length of the two gluons in nuclei before their fusion into a charmonium at  $\mathbf{x}$ ,  $z_A$  and  $z_B$  are the longitudinal coordinates of the two nucleons where the two gluons come from,  $a_{gN}$  is the averaged charmonium transverse momentum square obtained from the gluon scattering with a unit of length of nucleons, and  $f_{\Psi}^{pp}(\mathbf{p})$  is the momentum distribution for a free p+p collision. The length  $l$  is calculated from the nuclear geometry, and the Cronin parameter  $a_{gN}$  is usually extracted from corresponding p+A collisions where the produced charmonia suffer from only cold nuclear matter effect. Considering the absence of p+A data at LHC energy, we take  $a_{gN} = 0.15 \text{ GeV}^2/\text{fm}$  from empirical estimations [47–49].

Assuming that the emitted gluon in the gluon fusion process  $g + g \rightarrow \Psi + g$  is soft in comparison with the initial gluons and the produced charmonium and can be neglected in kinematics, corresponding to the picture of color evaporation model at leading order [50–52], the longitudinal momentum fractions of the two initial gluons are calculated from the momentum conservation,

$$x_{1,2} = \frac{\sqrt{m_{\Psi}^2 + p_T^2}}{\sqrt{s_{NN}}} e^{\pm y}, \quad (8)$$

where  $y$  is the charmonium rapidity. The free distribution  $f_{\Psi}^{pp}(\mathbf{p})$  can be obtained by integrating the elementary partonic processes,

$$\frac{d\sigma_{\Psi}^{pp}}{dp_T dy} = \int dy_g x_1 x_2 f_g(x_1, \mu_F) f_g(x_2, \mu_F) \frac{d\sigma_{gg \rightarrow \Psi g}}{d\hat{t}}, \quad (9)$$

where  $f_g(x, \mu_F)$  is the gluon distribution in a free proton,  $y_g$  is the emitted gluon's rapidity,  $d\sigma_{gg \rightarrow \Psi g}/d\hat{t}$  is the charmonium

momentum distribution produced from a fusion process, and  $\mu_F$  is the factorization scale of the fusion process.

Now we consider the shadowing effect. The distribution function  $\bar{f}_i(x, \mu_F)$  for parton  $i$  in a nucleus differs from a superposition of the distribution  $f_i(x, \mu_F)$  in a free nucleon. The nuclear shadowing can be described by the modification factor  $R_i = \bar{f}_i/(A f_i)$ . To account for the spatial dependence of the shadowing in a finite nucleus, one assumes that the inhomogeneous shadowing is proportional to the parton path length through the nucleus [53], which amounts to consider the coherent interaction of the incident parton with all the target partons along its path length. Therefore, we replace the homogeneous modification factor  $R_i(x, \mu_F)$  by an inhomogeneous one  $\mathcal{R}_i(x, \mu_F, \mathbf{x})$  [54]

$$\mathcal{R}_i = 1 + A(R_i - 1) T_A(\mathbf{x}_T)/T_{AB}(0) \quad (10)$$

with the definition  $T_{AB}(\mathbf{b}) = \int d^2\mathbf{x}_T T_A(\mathbf{x}_T) T_B(\mathbf{x}_T - \mathbf{b})$ . We employ in the following the EKS98 package [23] to evaluate the homogeneous ratio  $R_i$ , and the factorization scale is taken as  $\mu_F = \sqrt{m_{\Psi}^2 + p_T^2}$ .

Replacing the free distribution  $f_g$  in (9) by the modified distribution  $\bar{f}_g = A f_g \mathcal{R}_g$  and taking into account the Cronin effect (7), we finally get the initial charmonium distribution for the transport equation (3),

$$\begin{aligned} f_{\Psi}(\mathbf{x}, \mathbf{p}, \tau_0|\mathbf{b}) &= \frac{(2\pi)^3}{E_T \tau_0} \int dz_A dz_B \rho_A(\mathbf{x}_T, z_A) \rho_B(\mathbf{x}_T, z_B) \\ &\times \mathcal{R}_g(x_1, \mu_F, \mathbf{x}_T) \mathcal{R}_g(x_2, \mu_F, \mathbf{x}_T - \mathbf{b}) \\ &\times \bar{f}_{\Psi}^{pp}(\mathbf{x}, \mathbf{p}, z_A, z_B|\mathbf{b}), \end{aligned} \quad (11)$$

where  $\rho_A$  and  $\rho_B$  are the nucleon distribution functions in the two colliding nuclei. Now the only thing left is the distribution  $f_{\Psi}^{pp}$  in a free p+p collision which can be fixed by data or by some empirical estimations.

Since the charmonia in heavy ion collisions at LHC are measured by the CMS collaboration at mid rapidity  $|y| < 2.4$  [18, 20] and by the ALICE collaboration at mid rapidity  $|y| < 0.9$  [19, 55] and forward rapidity  $2.5 < y < 4$  [56–58], one should consider the rapidity dependence of the free distribution  $f_{\Psi}^{pp}$ . The charmonium states measured by the ALICE are reconstructed down to  $p_T = 0$  via the  $\mu^+ \mu^-$  decay channel at forward rapidity and via the  $e^+ e^-$  channel at mid rapidity. From the measurement [59], the averaged cross section is  $d\sigma_{\Psi}^{pp}/dy = 4.1 \mu\text{b}$  at  $|y| < 0.9$  and  $2.3 \mu\text{b}$  at  $2.5 < y < 4$ . The ALICE has also measured the transverse momentum distribution in p+p collisions [59], the combined  $y$  and  $p_T$  dependence for inclusive  $J/\psi$ s at  $2.5 < y < 4$  can be parameterized as

$$\frac{d^2\sigma_{\Psi}^{pp}}{dy p_T dp_T} = \frac{2(n-1)}{(n-2)\langle p_T^2 \rangle_{pp}} \left( 1 + \frac{p_T^2}{(n-2)\langle p_T^2 \rangle_{pp}} \right)^{-n} \frac{d\sigma_{\Psi}^{pp}}{dy} \quad (12)$$

with  $n = 5.06$  and  $\langle p_T^2 \rangle_{pp} = 7.8(\text{GeV}/c)^2$ , shown as the lower solid line in Fig.1. From the ALICE [60] and RHIC [61] data and CEM(Color Evaporation Model) [62] calculation, the free distribution  $d^2\sigma_{\Psi}^{pp}/(dy p_T dp_T)$  for inclusive  $J/\psi$ s at rapidity  $|y| < 2.4$  can also be described by the parametrization (12)

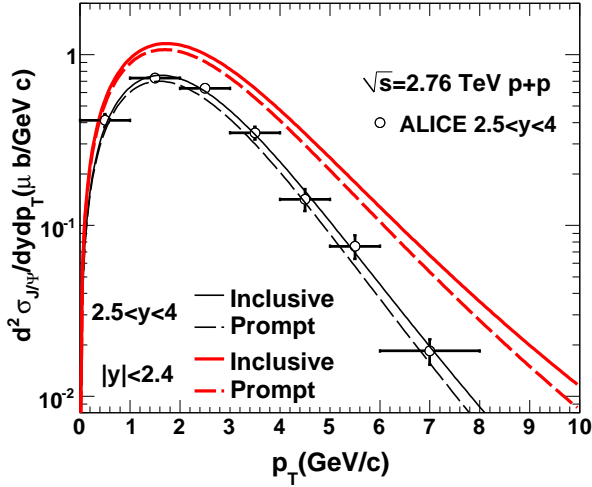


FIG. 1: (color online) The parametrization of inclusive (solid line) and prompt (dashed line)  $J/\psi$  production cross section as a function of transverse momentum in 2.76 TeV p+p collisions. The thick-(red online) and thin-(black online) lines represent mid-rapidity and forward-rapidity, respectively. The data at forward-rapidity are from the ALICE Collaboration [59].

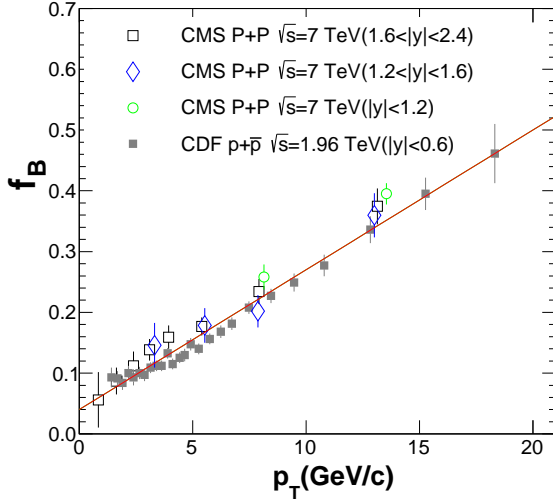


FIG. 2: (color online) The B decay fraction as a function of  $J/\psi$  transverse momentum in p+p collisions. The data are from the CDF [64] and CMS [65] collaborations, and the straight line is our linear parametrization.

with  $n = 4$ ,  $\langle p_T^2 \rangle_{pp} = 10 \text{ (GeV/c)}^2$  and  $d\sigma_{\psi}^{pp}/dy = 4.1 \mu\text{b}$ , see the other solid line in Fig.1.

The inclusive  $J/\psi$ s measured by ALICE include the prompt part and the contribution from the B decay. The former consists of direct production and feed down from the excited states, 30% from  $\chi_c$  and 10% from  $\psi'$ , and the latter comes from the decay of bottomed hadrons. The B decay contributes about 10% [63–65] to the total inclusive yield. Since the ALICE does not separate the two parts from each other, we

have to take into account the B decay contribution in our model to compare our theoretical calculation with the ALICE data. CMS experiment has measured the prompt charmonia at high transverse momentum  $6.5 < p_T < 30 \text{ GeV/c}$  and at mid-rapidity  $|y| < 2.4$  [18]. Since at the moment there are no p+p data for prompt charmonia in the CMS rapidity region, we employ  $d\sigma_{\psi}^{pp}/dy = 4.1 \mu\text{b}$  from the ALICE data [59] for inclusive  $J/\psi$ s in mid-rapidity, and then eliminate the B decay contribution by multiplying the inclusive cross section by a factor of  $(1 - f_B(p_T))$ , where  $f_B$  is the B decay fraction. Fig.2 shows the recent data on the B decay fraction in p+p( $\bar{p}$ ) collisions as a function of  $J/\psi$   $p_T$  [65]. The data can be well parameterized as  $f_B(p_T) = 0.04 + 0.023 p_T / (\text{GeV/c})$ . Note that the linear parametrization is rapidity independent in the region we considered. The prompt  $J/\psi$  distribution at mid-rapidity  $|y| < 2.4$  is shown as the upper dashed curve in Fig.1. Since the B decay fraction is approximately rapidity independent, the distribution  $f_{\psi}^{pp}$  for inclusive  $J/\psi$ s at mid-rapidity  $|y| < 0.9$  can be obtained from the prompt distribution at mid-rapidity  $|y| < 2.4$  and the B decay fraction  $f_B$  shown in Fig.2.

We now turn to the rapidity dependence of the charm quark production cross section  $\sigma_{c\bar{c}}^{pp}$  in (6). From the ALICE data [42], there is  $d\sigma_{c\bar{c}}^{pp}/dy = 0.65 \text{ mb}$  at mid-rapidity. By taking the FONLL [43, 44] scaling, we extract  $d\sigma_{c\bar{c}}^{pp}/dy = 0.4 \text{ mb}$  at forward-rapidity. Considering the uncertainty in the experimental data and theoretical calculations (see Fig.5 of Ref.[42]), the upper limits of FONLL [44] and pQCD are often used in models [45], to estimate the maximum quarkonium production. We take in the following numerical calculations  $d\sigma_{c\bar{c}}^{pp}/dy$  between 0.65 and 0.8 mb at mid-rapidity and 0.4 and 0.5 mb at forward-rapidity. Note that the shadowing effect changes not only the initial  $J/\psi$  distribution, but also the in-medium  $J/\psi$  regeneration and the non-prompt contribution from the B decay, by reducing the number of charm and bottom quarks. In principle, the shadowing should be centrality dependent. To simplify the numerical calculations, we take in the following a reduction of 20% for the charm and bottom quark production cross sections, estimated from the centrality averaged EKS98 evolution [23].

## IV. NUMERICAL RESULTS

### A. Centrality Dependence of $R_{AA}$

We start with the  $J/\psi$  nuclear modification factor  $R_{AA} = N_{AA} / (N_{coll} N_{pp})$  as a function of the number of participants  $N_{part}$ , where  $N_{pp}$  and  $N_{AA}$  are respectively the numbers of measured  $J/\psi$ s in p+p and A+A collisions, and  $N_{coll}$  is the number of nucleon-nucleon collisions at fixed  $N_{part}$ . Our model calculations for 2.76 TeV Pb+Pb collisions and the comparison with the inclusive ALICE data are shown in Fig.3 at forward-rapidity (upper panel) and mid-rapidity (lower panel).

With increasing centrality, the initial contribution (dot-dashed lines) drops down and the regeneration (dashed lines) goes up monotonously. Considering the uncertainty in the charm quark production cross section, we take the range of



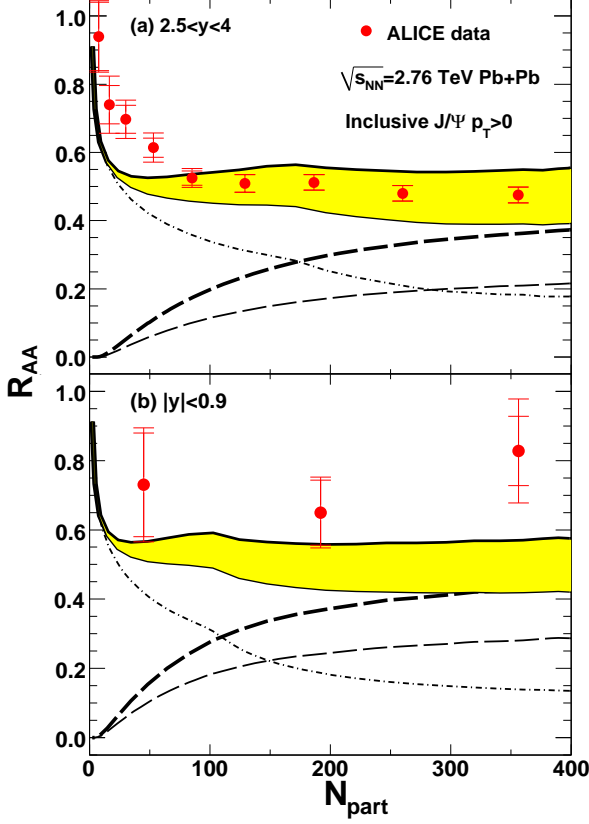


FIG. 3: (color online) The  $J/\psi$  nuclear modification factor as a function of centrality for 2.76 TeV Pb+Pb collisions at forward rapidity (upper panel) and mid rapidity (lower panel). The dot-dashed lines represent the initial fraction. The thick and thin dashed lines represent the regeneration fraction with the upper and lower limits of charm quark cross-sections  $d\sigma_{cc}^{pp}/dy = 0.8$  and  $0.65$  mb at mid rapidity and  $0.5$  and  $0.4$  mb at forward rapidity. The hatched bands represent the full results. The data points are taken from ALICE experiment [59].

cross-sections  $d\sigma_{cc}^{pp}/dy = 0.4$  and  $0.5$  mb at forward rapidity and  $0.65$  and  $0.8$  mb at midrapidity, corresponding to the thin and thick dashed lines in Fig.3. This uncertainty in the regeneration results in a band for the full result. Different from the collisions at SPS energy where the regeneration can be neglected [10, 24] and at RHIC energy where the initial production is still a dominant component and the regeneration becomes equivalently important only in very central collisions [12, 66], the regeneration at LHC energy becomes the dominant source of charmonium production in a wide centrality bin. The competition between the strong dissociation and regeneration leads to a flat structure for the total charmonium production at both forward rapidity and mid rapidity, see Fig.3. At forward rapidity where high statistic data are available, our model results well explain the data in semi-central and central collisions with  $N_{part} \gtrsim 100$ , and the deviation from the data in small  $N_{part}$  region is probably due to the invalidation of hydrodynamics for the medium and the canonical

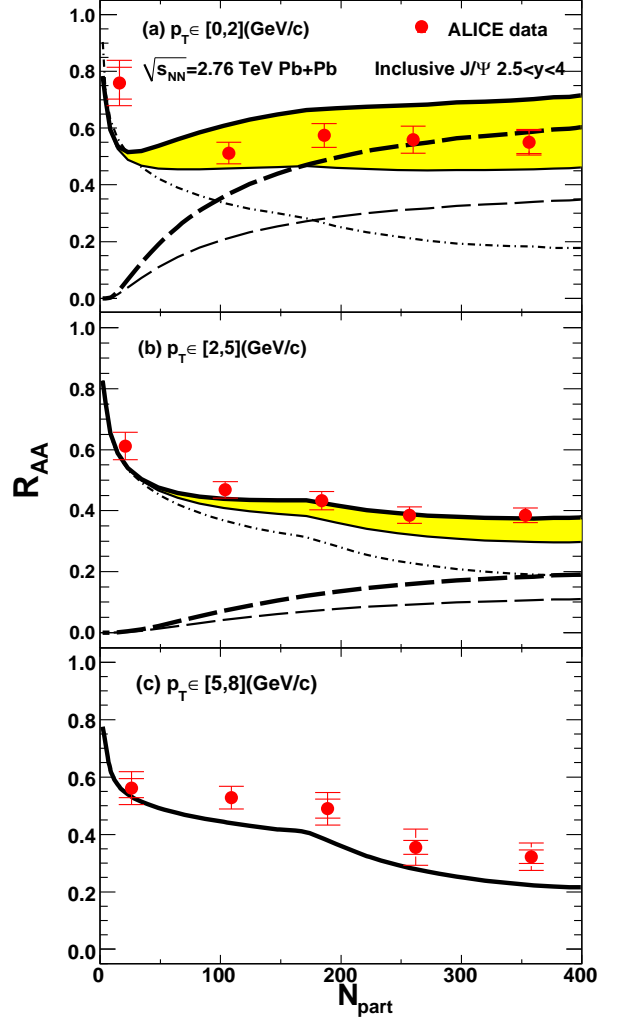


FIG. 4: (color online) The  $J/\psi$  nuclear modification factor as a function of centrality for 2.76 TeV Pb+Pb collisions at forward rapidity and in different transverse momentum bins. The dot dashed lines are the initial fraction, the thick and thin dashed lines are the regeneration fraction with charm quark cross section  $d\sigma_{cc}^{pp}/dy = 0.5$  and  $0.4$  mb, and the bands are the full result. The data are from the ALICE collaboration [21].

limit for the charmonium regeneration [67, 68]. At mid rapidity where the data are with large error bars, the model results seem systematically under the data.

We have seen the strong competition between the charmonium suppression and regeneration in the centrality dependence of the  $J/\psi$  yield. In order to see the charmonium production and suppression mechanisms more clearly in heavy ion collisions, we turn to the transverse momentum dependence of the yield. Figs.4 and 5 show the nuclear modification factor  $R_{AA}$  as a function of centrality in different  $p_T$  bins. In addition we make comparisons with ALICE data [21] (Fig.4) and CMS data [18] (Fig.5) for inclusive and prompt  $J/\psi$  production, respectively.

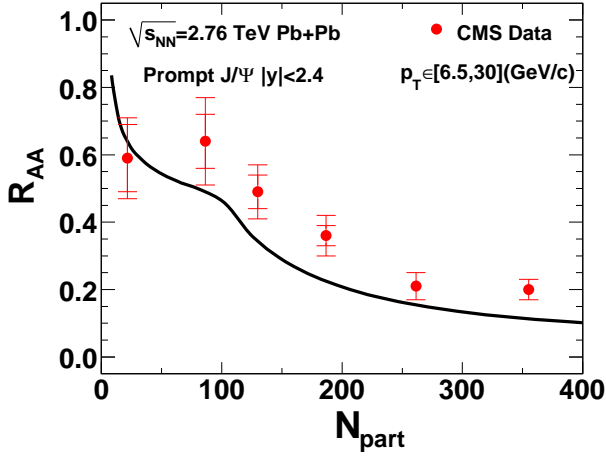


FIG. 5: (color online) The  $J/\psi$  nuclear modification factor as a function of centrality for 2.76 TeV Pb+Pb collisions at mid rapidity and in a high transverse momentum bin. The line is the model calculation and the data are from the CMS collaboration [18].

In our calculation, we considered a reduction of 20% for the charm quark number due to the strong shadowing effect at LHC energy. We also took a kinetically thermalized charm quark distribution, by assuming strong interaction between charm quarks and the medium. For bottom quarks, we took into account the same reduction for the number in the calculation of  $p_T$  integrated yield. Since bottom quarks are so heavy, their thermalization is unreasonable in nuclear collisions. While the total  $J/\psi$  yield shown in Fig.3 is not sensitive to the bottom quark transverse momentum distribution, it may change remarkably the  $J/\psi$  yield in a fixed  $p_T$  bin, especially in a high  $p_T$  bin where the bottom quark energy loss becomes important. Inspired from the CMS measurement [20], we apply a B quench factor  $R_{AA}^B = 0.4$  when calculating the non-prompt  $J/\psi$ s in the region of  $5 < p_T < 8$  GeV/c.

Heavy quarks are produced via hard scatterings and their initial momentum distribution is hard. Through interaction with the medium, heavy quarks lose energy, and the corresponding  $p_t$  distribution becomes steeper. Since the medium is hot and dense, some of the charm quarks are even thermalized. Considering that the regenerated charmonia from thermalized charm quarks in hot medium are mainly distributed in low momentum region, their contribution to the yield decreases with increasing transverse momentum, and therefore the band structure for the total result due to the uncertainty in regeneration disappears in the high  $p_T$  bins  $5 < p_T < 8$  GeV/c and  $6.5 < p_T < 30$  GeV/c, see Figs.4 and 5. As we have pointed out that the flat platform for semi-central and central collisions comes from the competition between the suppression and regeneration, it vanishes in the high  $p_T$  bins due to the disappearance of the regeneration. The yield in high  $p_T$  bins is characterized by the Debye screening effect on the initially produced charmonia. In this case, there exists a kink for the nuclear modification factor which is located at  $N_{part} \sim 200$  (Fig.4) for  $5 < p_T < 8$  GeV/c at forward ra-

pidity and  $N_{part} \sim 100$  (Fig.5) for  $6.5 < p_T < 30$  GeV/c in mid rapidity. Before the kink, the temperature of the fireball is less than the  $J/\psi$  dissociation temperature  $T_{J/\psi}$  and there is  $R_{AA} \sim 0.6$ , resulted from the fact that the decay contribution from the excited charmonium states to the finally observed  $J/\psi$ s is about 40%. Starting at the kink, the temperature is higher than  $T_{J/\psi}$  and the  $J/\psi$  suppression becomes more and more important in more central collisions. As one can see from Figs.4 and 5, the kink at mid rapidity appears at a lower value of  $N_{part}$  than that at forward-rapidity. This is due to the fact that the medium at mid rapidity is hotter and  $J/\psi$  starts to melt at more peripheral collisions. The model results underestimate the high  $p_T$  results a bit, see Figs.4 and 5. Part of the discrepancy may due to the fact we have not include the velocity dependence of the dissociation temperature. As discussed in [69], fast moving charmonia tend to be melt at a higher temperature making the velocity dependence particularly important in high  $p_T$  regions.

### B. Transverse Momentum Dependence of $R_{AA}$

The transverse momentum distribution of the nuclear modification factor  $R_{AA}(p_T)$  in a fixed centrality bin and its comparison with the ALICE data are shown in Fig.6 for inclusive  $J/\psi$ s at forward rapidity. We see clearly that, the regeneration (dashed lines) dominants the low  $p_T$  regions at all centralities. On the other hands, initially produced  $J/\psi$ s (dot-dashed lines) become important at high  $p_T$  region. Therefore, the competition between the suppression and regeneration depends strongly on the transverse momentum and collision centralities. When both the regeneration at low  $p_T$  and initial production at high  $p_T$  are important, there exists a minimum structure located at intermediate  $p_T$ , see the upper and middle panels of Fig.6. Note that without the regeneration as the second production source, the nuclear modification factor  $R_{AA}$  would decrease monotonously with increasing centrality and increases monotonously with increasing transverse momentum. The  $R_{AA}(p_T)$  for prompt  $J/\psi$ s at mid rapidity is shown in Fig.7. While the CMS data are in the high  $p_T$  region where there is almost no contribution from the regeneration and the system is controlled only by the dissociation of the initially produced  $J/\psi$ s, the predicted  $R_{AA}$  at very low  $p_t$  is larger than unity which is not possible without the regeneration mechanism.

### C. A New Ratio $r_{AA} = \langle p_T^2 \rangle_{AA} / \langle p_T^2 \rangle_{pp}$

For heavy ion collisions in the past decades, the colliding energy from SPS to LHC increases by two orders of magnitude, and the heavy quark production cross section increases dramatically. While the transverse momentum dependence of the nuclear modification factor  $R_{AA}$  tells us the importance of the regeneration mechanism, we hope to find a quantity which is more sensitive to the nature of the medium. On the other hand, in our treatment for hot nuclear matter effect, we assumed a thermalized charm quark distribution for the calcula-

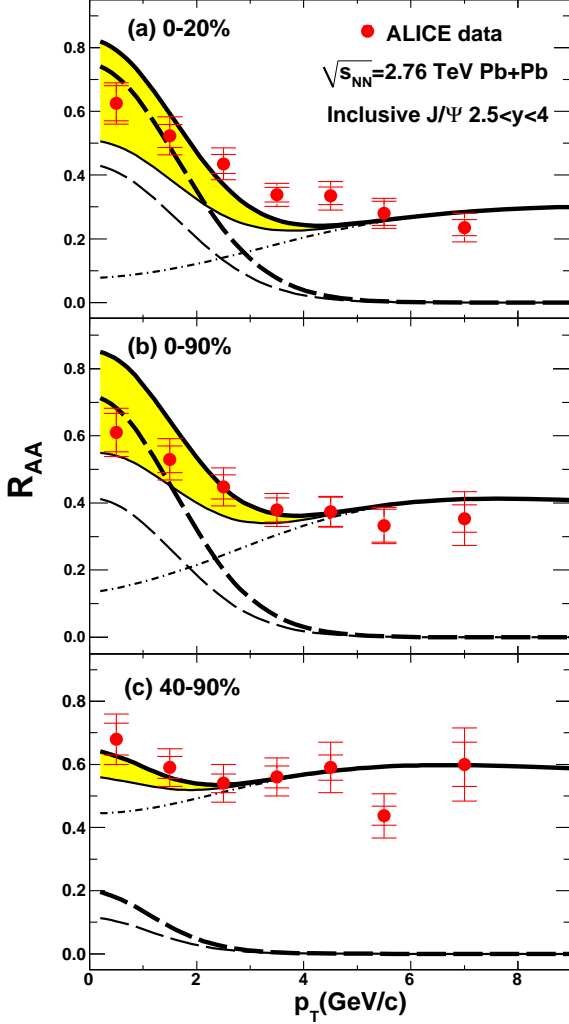


FIG. 6: (color online) The  $J/\psi$  nuclear modification factor as a function of transverse momentum for 2.76 TeV Pb+Pb collisions at forward rapidity and in different centrality bins. The dot-dashed lines are the initial fraction, the thick and thin dashed lines are the regeneration fraction with charm quark cross section  $d\sigma_{cc}^{pp}/dy = 0.5$  and  $0.4$  mb, and the bands are the full result. The data are from the ALICE collaboration [21].

tion of the regeneration rate, how good is this assumption and how does the charm quark thermalization affect the charmonium distribution? The other question is how to separate the hot nuclear matter effect from the cold nuclear matter effect. To focus on the property of the hot medium, we hope to have a quantity which is sensitive to the hot nuclear matter effect but affected weakly by the cold nuclear matter effect. To these ends, we introduced a new nuclear modification factor for the transverse momentum [70]

$$r_{AA} = \frac{\langle p_T^2 \rangle_{AA}}{\langle p_T^2 \rangle_{pp}}, \quad (13)$$

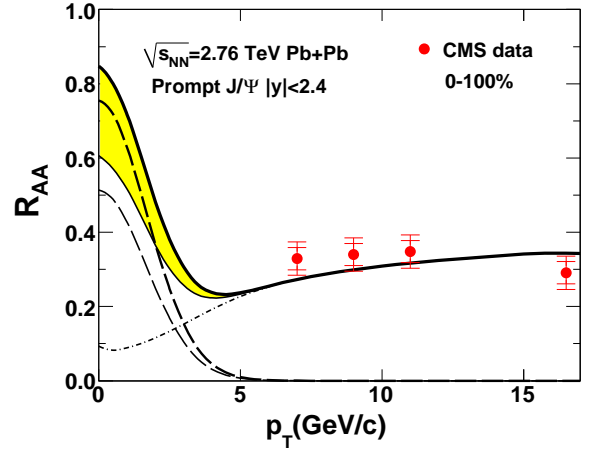


FIG. 7: (color online) The  $J/\psi$  nuclear modification factor as a function of transverse momentum for 2.76 TeV Pb+Pb collisions at mid-rapidity and in minimum bias event. The dot-dashed line is the initial fraction, the thick and thin dashed lines are the regeneration fraction with charm quark cross section  $d\sigma_{cc}^{pp}/dy = 0.8$  and  $0.65$  mb, and the band is the full result. The data are from the CMS collaboration [20].

where  $\langle p_T^2 \rangle_{AA}$  and  $\langle p_T^2 \rangle_{pp}$  are averaged transverse momentum square for  $J/\psi$  in A+A and p+p collisions, respectively. To be different from the usually used nuclear modification factor  $R_{AA}$  for the yield, we take here  $r_{AA}$  as the ratio of the second moment of transverse momentum distributions. Since the nuclear matter effect changes not only the size of the transverse momentum but also its shape, we focus on  $\langle p_T^2 \rangle$  instead of  $\langle p_T \rangle$ . It is worthy to note that the second moment of the  $p_T$  distribution is also sensitive to the Cronin effect but not much affected by the parton distribution functions. The calculation and the comparison with experimental data at SPS, RHIC and LHC energies are shown in Fig.8 for two rapidity bins. In mid-rapidity where the hot nuclear matter effect is most important, the ratio changes significantly with increasing colliding energy,

$$r_{AA} \begin{cases} > 1 & \text{SPS} \\ \sim 1 & \text{RHIC} \\ < 1 & \text{LHC} \end{cases} \quad \text{at mid-rapidity,} \quad (14)$$

see the upper panel of Fig.8. At SPS, almost all the measured  $J/\psi$ s are produced through initial hard processes and carry high momentum. The continuous increasing with centrality arises from the Cronin effect and leakage effect [24]. The latter is described by the third term on the left hand side of the transport equation (3) and means that the high  $p_T$   $J/\psi$ s can escape from the hot medium. At RHIC, the regeneration starts to play a role and even becomes equally important as the initial production in central collisions [12, 66], the cancelation between the suppression and regeneration leads to a flat  $r_{AA}$  around unity. At LHC, the regeneration becomes dominant, especially in central collisions. Since the regenerated charmonia carry low momentum in comparison with the initial production, the more and more important regeneration results in a decreasing  $r_{AA}$  with increasing centrality. This tremen-

dous change in the  $p_T$  ratio comes from the nature of the hot medium at each corresponding collision energy. Our calculation agrees well with the data at SPS and RHIC energies. At LHC energy there are currently no data at mid rapidity. The band structure at LHC is again from the uncertainty in the charm quark production cross section. Note that, different from the ratio  $R_{AA}$  for the yield where the lower and higher borders of the band correspond to the smaller and larger cross sections, the relation between the two borders of  $r_{AA}$  and the cross section is in an opposite way, namely, the lower and higher borders here correspond to the larger and smaller cross sections. Intuitively this is simple to understand: In the case of larger charm quark cross section, more  $J/\psi$ s are from the regeneration and then carry low momentum. To have a comparison with the LHC data, we calculated the ratio  $r_{AA}$  in the forward rapidity where the hot medium effect becomes weaker. In this case the trend of the ratio is still very different at RHIC and LHC: With increasing centrality it goes up at RHIC but drops down at LHC.

$$r_{AA} \begin{cases} > 1 & \text{RHIC} \\ < 1 & \text{LHC} \end{cases} \quad \text{at forward rapidity,} \quad (15)$$

see the lower panel of Fig.8. The calculation agrees well with both the RHIC and LHC data.

After a careful inspecting the centrality dependence of  $r_{AA}$ , one can find a common feature in all cases, namely,  $r_{AA}$  in peripheral collisions is always increasing as the centrality increases. In case the initial production is dominant, the ratio continues to increase, while strong regeneration from thermalized charm quarks pulls the ratio down below unity in more central collisions. In order to see if charm quarks are thermalized with the hot medium, we calculate now the ratio  $r_{AA}$  at LHC energy with a pQCD simulated charm quark distribution, shown in the upper panel of Fig.9 at forward rapidity. The thermal distribution is the limit of strong interaction between charm quarks and the medium, while the pQCD distribution taken from the simulator PYTHIA [73] is the limit of no interaction. For the pQCD distribution, the charm quark energy loss is excluded, the initially produced charm quarks keep their high momentum in the medium, and therefore the regenerated charmonia will be no longer soft but carry high momentum. In this case, the averaged transverse momentum is enhanced at the forward rapidity and the ratio  $r_{AA}$  becomes larger than the one with thermal distribution, see the upper panel of Fig.9. Again the band is due to the uncertainty in the charm quark cross section. From the comparison with the ALICE data, we conclude that charm quarks are thermalized in high-energy nuclear collisions at the LHC energy.

In the above calculations we have taken a reduction of 20% for the charm and bottom quark distributions in the medium, due to the shadowing effect. This reduction leads to an extra charmonium suppression. Supposing the total number of initially produced charm quarks is  $n_c$ , the regenerated charmonium number is then proportional to  $n_c^2$  if we do not take into account the shadowing effect and  $(0.8n_c)^2 = 0.64n_c^2$  when the shadowing effect is included. However, the averaged transverse momentum square  $\langle p_T^2 \rangle$  is a normalized quantity, it should not be so sensitive to the shadowing effect. The

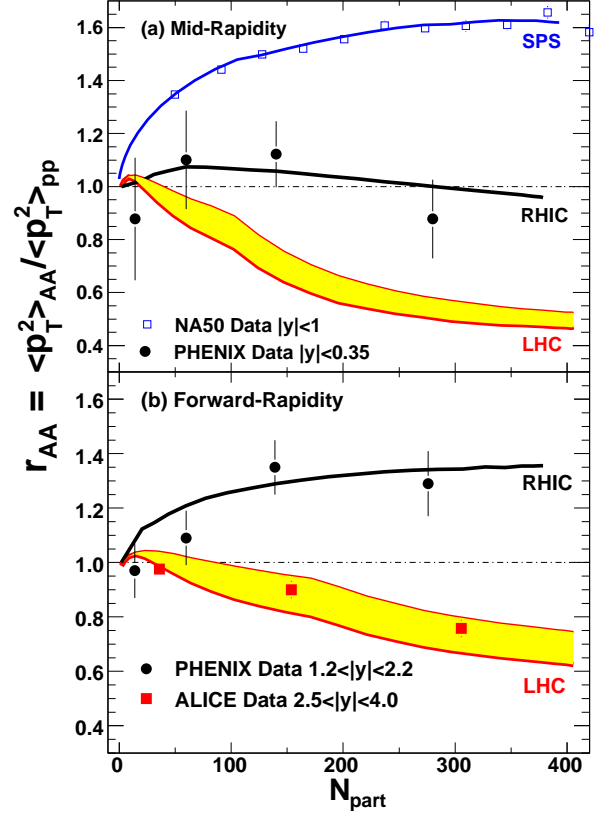


FIG. 8: (color online) The newly defined nuclear modification factor  $r_{AA} = \langle p_T^2 \rangle_{AA} / \langle p_T^2 \rangle_{pp}$  for  $J/\psi$ s as a function of centrality at SPS, RHIC and LHC energies. The bands at LHC are due to the uncertainty in the charm quark cross section  $0.4 < d\sigma_{cc}^{pp}/dy < 0.5$  mb at forward rapidity (lower panel) and  $0.65 < d\sigma_{cc}^{pp}/dy < 0.8$  mb at mid rapidity (upper panel), and the data are from NA50 [5], PHENIX [71] and ALICE [72] collaborations.

comparison between the calculations with and without considering the shadowing effect is shown in the lower panel of Fig.9. As we expected, the two bands are very close to each other and overlap partly. This indicates that the nuclear modification factor  $r_{AA}$  for charmonium transverse momentum can be used to extract the hot medium information with only small correction from the early shadowing effect.

#### D. Elliptic Flow $v_2$

Since the elliptic flow originates from the geometric anisotropy in the configuration space and develops in the evolution of the hot medium, it is significant in semi-central collisions and approaches to zero in peripheral and central collisions. As far as the charmonium concern, those that produced from the initial collisions prior to the formation of the hot medium will not present any significant elliptic flow, see the dot-dashed line in the upper panel of Fig.10. The regener-



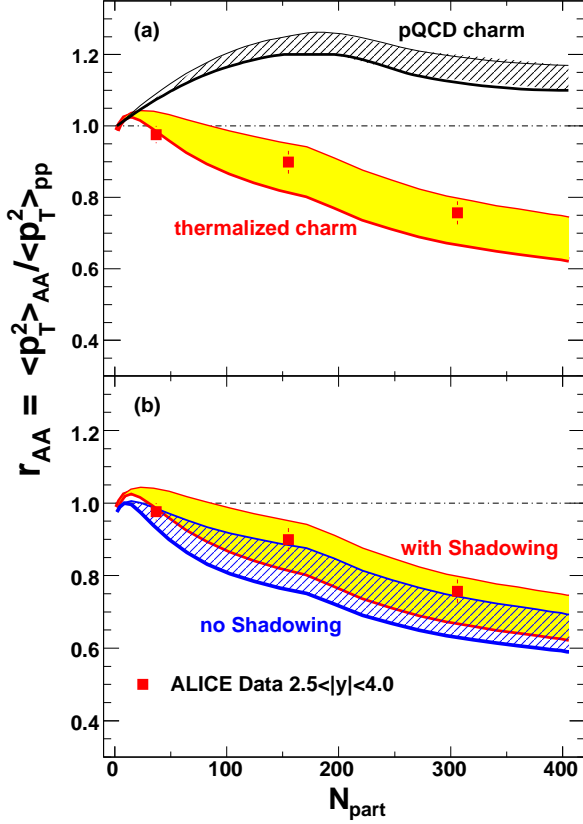


FIG. 9: (color online) The newly defined nuclear modification factor  $r_{AA} = \langle p_T^2 \rangle_{AA} / \langle p_T^2 \rangle_{pp}$  for  $J/\psi$  as a function of centrality at LHC energy and at forward rapidity. The upper and lower panels are the comparisons between pQCD and thermal charm quark distributions and between with and without shadowing effect. The bands are again due to the uncertainty in the charm quark cross section  $0.4 < d\sigma_{cc}^{pp}/dy < 0.5$  mb, and the data are from the ALICE collaboration [72].

ated  $J/\psi$ s, on the other hand, may inherit flow from the thermalized charm quarks, as shown by the dashed line. Through interactions, the initial anisotropy in the configuration space is converted into the anisotropy in momentum space for all final hadrons. The full  $J/\psi$   $v_2$  is shown as the solid line in the upper panel of Fig.10. Note that a sizable  $v_2$  has been developed at LHC. Unlike the light charged hadrons where  $v_2$  persist with large values up to high  $p_T$  region, the  $J/\psi$   $v_2$  quickly drops to the value from initial production with  $v_2 \leq 1\%$ .

Up to now, our discussion on  $J/\psi$   $v_2$  is focused on the prompt  $J/\psi$ . Once we include the  $J/\psi$  from bottom quark decay, new scenarios arise. The lower panel of Fig.10 shows the elliptic flow  $v_2$  for inclusive  $J/\psi$ s at forward rapidity where the bottom decay is included. As one can see in the plot, the  $J/\psi$   $v_2$  from the decay of the initially (or pQCD) produced bottom quarks quickly falls to close to zero at  $p_T \sim 5$  GeV/c. However, the  $J/\psi$ s from thermalized bottom decay show significant value of  $v_2$  at high  $p_T$  region. At this point, the error of the experimental data is too large to draw any conclusion of

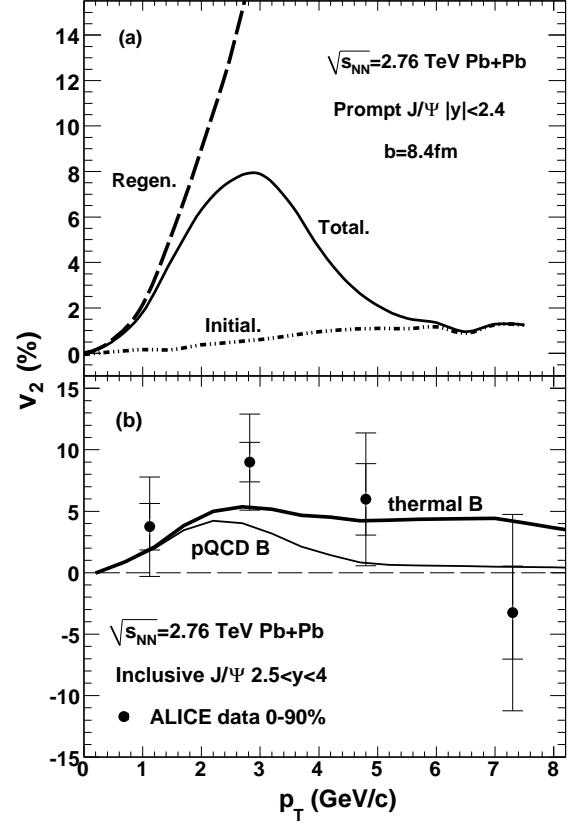


FIG. 10: (upper panel) The elliptic flow  $v_2$  for prompt (upper panel) and inclusive (lower panel)  $J/\psi$ s in  $\sqrt{s_{NN}} = 2.76$  TeV Pb+Pb collisions. The calculation is with impact parameter  $b = 8.4$  fm, corresponding to the minimum bias event. The dot-dashed, dashed and solid lines represent the initial, regeneration and total contributions. In the lower panel, the thick and thin lines indicate the total results including thermal bottom decay and pQCD bottom decay, respectively. The experimental data are taken from ALICE experiment [74].

bottom quark thermalization. Our calculation predicts that future precise  $J/\psi$   $v_2$  at high  $p_T$  will provide important information on bottom production in high energy nuclear collisions.

## V. CONCLUSION

We have studied the cold and hot nuclear matter effects on charmonium production in relativistic heavy ion collisions. In the framework of a transport approach for the charmonium motion plus a hydrodynamic description for the medium evolution, we calculated the charmonium transverse momentum distribution and the corresponding ratios  $R_{AA}$  and  $r_{AA}$  in different rapidity and centrality bins. Our model calculations agree reasonably well with the experimental data at SPS, RHIC and LHC energies. We found that, in comparison with the often used nuclear modification factor  $R_{AA} = N_{AA} / (N_{coll} N_{pp})$ , based on the charmonium yield, the newly defined nuclear

modification factor  $r_{AA} = \langle p_T^2 \rangle_{AA} / \langle p_T^2 \rangle_{pp}$ , based on the charmonium transverse momentum distribution, is more sensitive to the nature of the hot medium and to the degree of heavy quark thermalization. When the colliding energy increases from SPS to LHC, the  $p_T$   $r_{AA}$  changes dramatically from above unity and increasing as a function of collision centrality to below unity and decreasing versus centrality. Different from the yield  $R_{AA}$  which is strongly affected by both the cold and hot nuclear matter effects, the  $p_T$   $r_{AA}$  is weakly affected by the shadowing effect. In addition, we observed that the  $J/\psi$

elliptic flow  $v_2$  for minimum bias events evolves from almost zero at RHIC to a large value similar to that of light hadrons at LHC. The root for these observed dramatic changes is the formation of the strongly coupled quark-gluon plasma and the thermalization of charm quarks in high energy nuclear collisions at the LHC energy.

**Acknowledgement:** The work is supported by the NSFC, the MOST and the DOE grant Nos. 11221504, 11335005, 11275103, 2013CB922000, 2014CB845400, and DE-AC03-76SF00098.

- 
- [1] T.Matsui and H.Satz, Phys. Lett. **B178**, 416(1986).
  - [2] M.Asakawa and T.Hatsuda, Phys. Rev. Lett. **92**, 012001(2004)
  - [3] S.Datta, F.Karsch, P.Petreczky and I.Wetzorke, Phys. Rev. **D69**, 094507(2004).
  - [4] M.Gonin, et al., Nucl. Phys. **A610**, 404(1996).
  - [5] N.S.Topilskaya, et al., [NA50 Collaboration], Nucl. Phys. **A715**, 675(2003).
  - [6] B.Alessandro, et al.[NA50 Collaboration], Eur. Phys. J. **C39**, 335(2005).
  - [7] J.Adams, et al., [STAR Collaboration], Phys. Rev. Lett. **94**, 062301(2005).
  - [8] A.Adare, et al., [PHENIX Collaboration] Phys. Rev. Lett. **97**, 252002(2006).
  - [9] P.Braun-Munzinger and J.Stachel, Phys. Lett. **B490**, 196(2000); A.Adronic, P.Braun-Munzinger, K.Redlich and J.Stachel, Phys. Lett. **B652**, 259(2007).
  - [10] L.Grandchamp and R.Rapp, Nucl. Phys. **A709**, 415(2002).
  - [11] R.L.Thews M. Schroedter and J. Rafelski, Phys. Rev. **C63**, 054905(2001).
  - [12] L.Yan, P.Zhuang and N.Xu, Phys. Rev. Lett. **97**, 232301(2006).
  - [13] X.Zhao and R.Rapp, Phys. Lett. **B664**, 253(2008).
  - [14] A.H.Mueller and J.W.Qiu, Nucl. Phys. **B268**, 427(1986).
  - [15] J.W.Cronin, et al., Phys. Rev. **D11**, 3105(1975); J.Hufner Y.Kurihara and H.J.Pirner, Phys. Lett. **B215**, 218(1988).
  - [16] C.Gerschel and J.Hufner, Phys. Lett. **B207**, 253(1988).
  - [17] E.M.C.Abreu, et al., Phys. Lett. **B466**, 408(1999).
  - [18] C.Silvestre, et al., [CMS Collaboration], J. Phys. **G38**, 124033(2011).
  - [19] J.Wiechula, et al., [ALICE Collaboration], C12-05-27.2 Proceedings, arXiv:1208.6566.
  - [20] CMS Collaboration, CMS-PAS-HIN-12-014(2012).
  - [21] D.Das, et al., [ALICE Collaboration], Conf. Proc.**57**, 37(2012), arXiv:1212.2704.
  - [22] C.Lourenco, H.K.Wöhri, Physics Reports **433**, 127(2006).
  - [23] K.J.Eskola, V.J.Kolhinen and C.A.Salgado, Eur. Phys. J. **C9**, 61(1999).
  - [24] X.Zhu, P.Zhuang and N.Xu, Phys. Lett. **B607**, 107(2005).
  - [25] J.Sollfrank, et al., Phys. Rev. **C55**, 392(1997).
  - [26] K.Hagiwara, et al., Particle Data Group, Phys. Rev. **D66**, 010001(2002).
  - [27] T.Hirano, H.Pasi and N.Yasushi, Phys. Rev. **C83**, 021902(2011).
  - [28] K.Gulbrandsen, [ALICE Collaboratoin], J. Phys. Conf. Ser. **446**, 012027(2013).
  - [29] A.Zoccoli, et al., HERA-B Collaboration, Eur. Phys. J. **C43**, 179(2005).
  - [30] J.Hufner and P.Zhuang, Phys. Lett. **B559**, 193(2003).
  - [31] G.Bhanot and M.E.Peskin, Nucl. Phys. **B156**, 365(1979); G.Bhanot and M.E.Peskin, Nucl. Phys. **B156**, 391(1979).
  - [32] F.Arleo, et al., Phys. Rev. **D65**, 014005(2002).
  - [33] YS.Oh, S.Kim and S.H.Lee, Phys. Rev. **C65**, 067901(2002).
  - [34] X.N.Wang, Phys. Lett. **B540**, 62(2002).
  - [35] H.Satz, J. Phys. **G32**, R25(2006).
  - [36] L.Kluberg and H.Satz, Helmut, arXiv:0901.3831[hep-ph], Relativistic Heavy Ion Physics, Landolt-Brnstein - Group I Elementary Particles, Nuclei and Atoms **23**, 373(2010).
  - [37] B.I.Abelev, et al., [STAR Collaboration ], Phys. Rev. Lett. **98**, 192301(2007).
  - [38] A.Dainese, [ALICE Collaboration], Pos. ICHEP2012, 417(2013), arXiv:1212.0995; Z.Conesa del Valle, [ALICE Collaboration], arXiv:1210.2163[nucl-ex], C12-05-27.2 Proceedings.
  - [39] A.Adare, et al., [PHENIX Collaboration ], Phys. Rev. Lett. **98**, 172301(2007).
  - [40] Z.Conesa del Valle, [ALICE Collaboration], Nucl. Phys. **A904-905**, 178c(2013); Bianchin, Chiara, et al., [ALICE Collaboration], arXiv:1111.6886[hep-ex], SQM 2011 Conference Proceedings.
  - [41] M.L.Miller, et al., Ann. Rev. Nucl. Part. Sci. **57**, 205(2007).
  - [42] B.Abelev, et al., [ALICE Collaboration], JHEP **07**, 191(2012).
  - [43] M.Cacciari, M.Greco, and P.Nason, JHEP, 9805:007(1998).
  - [44] M.Cacciari, S.Frixione, and P.Nason, JHEP, 0103:006(2001).
  - [45] X.Zhao and R.Rapp, Nucl. Phys. **A859**, 114(2011); X.Zhao, E.Andrew, R.Rapp, Nucl. Phys. **A904-905**, 611c(2013).
  - [46] Y.Liu, et al., Phys. Lett. **B697**, 32(2011).
  - [47] X.N.Wang, Phys. Rev. Lett. **81**, 2655(1998).
  - [48] R.Vogt, Int. J. Mod. Phys. **E12**, 211(2003).
  - [49] R.L.Thews and M.L.Mangano, Phys. Rev. **C73**, 014904(2006).
  - [50] H. Fritzsch, Phys. Lett. **B67**, 217(1977).
  - [51] J.F Amundson, et al., Phys. Lett. **B372**, 127(1996).
  - [52] J.F Amundson, et al., Phys. Lett. **B390**, 323(1997).
  - [53] S.R.Klein and R.Vogt, Phys. Rev. Lett. **91**, 142301(2003).
  - [54] R.Vogt, Phys. Rev. **C71**, 054902(2005).
  - [55] I.C.Arsene, et al., [ALICE Collaboration], Nucl. Phys. **A904-905**, 623c(2013).
  - [56] G.M.Garca, et al., [ALICE Collaboration], J. Phys. **G38**,124034(2011).
  - [57] P.Pillot, et al., [ALICE Collaboration], J. Phys. **G38**,124111(2011).
  - [58] D.Das, et al., [ALICE Collaboration], Pramana**79**, 863(2012).
  - [59] Pereira Da Costa Hugo , et al., [ALICE Collaboration], arXiv:1110.1035, AIP Conf. Proc.**1441**, 859(2012).
  - [60] B.Alessandro, et al., [ALICE Collaboration], J. Phys. **G32**, 1295(2006).
  - [61] S.S.Adler, et al., [PHENIX Collaboration], Phys. Rev. Lett. **92**, 051802(2004).

- [62] A.Accardi, et al., CERN-2004-009-A, HIP-2003-40/TH.
- [63] R.Aaij, et al., [LHCb Collaboration], Eur. Phys. J **C71**, 1645(2011).
- [64] D.Acosta, et al., [CDF Collaboration], Phys. Rev. **D71**, 032001(2005).
- [65] V.Khachatryan, et al., [CMS Collaboration], Eur. Phys. J. **C71**, 1575(2011).
- [66] Y.Liu, et al., J. Phys. **G36**, 064057(2009).
- [67] L.Grandchamp and R.Rapp, Phys. Lett. **B523**, 60(2001).
- [68] C.M.Ko, et al., Phys. Rev. Lett. **86**, 5438(2001).
- [69] Y.Liu, N.Xu and P.Zhuang, Phys. Lett. **B724**, 73(2013).
- [70] K.Zhou, N.Xu and P.Zhuang, Nucl. Phys. **A834**, 249(2010).
- [71] A.Adare, et al., [PHENIX Collaboration], Phys. Rev. Lett. **98**, 232301(2007).
- [72] E.Scomparin (INFN Torino), [ALICE Collaboration], QM2012 presentation.
- [73] T. Sjöstrand, et al., Comput. Phys. Commun **135**, 238(2001).
- [74] H.Yang, [ALICE Collaboration], Nucl. Phys. **A904-905**, 673c(2013).